PICTURE OF THE MONTH

Photographic Documentation and Environmental Analysis of an Intense, Anticyclonic Supercell on the Colorado Plains

ROGER EDWARDS

Storm Prediction Center, Norman, Oklahoma

STEPHEN J. HODANISH

National Weather Service, Pueblo, Colorado

(Manuscript received 6 February 2006, in final form 12 May 2006)

ABSTRACT

Anticyclonic left-moving supercells are observed each year in the United States, emanating both discretely and from storm splitting processes. Such thunderstorms often produce severe hail and wind gusts and, on rare occasion, tornadoes. The body of documentary literature on this subset of supercells is relatively scant compared with right-moving storms, and this is especially true regarding visual characteristics and conceptual models. Here a characteristic example of the anticyclonic supercell is presented using an intense and well-defined specimen that passed over Aroya, Colorado, on 15 June 2002. Photographic and radar documentation is provided in original and mirrored forms, for aid in conceptualizing the left-moving supercell and associated structures and processes. A summary overview is presented of the environment, development, evolution, and effects of this remotely located but noteworthy event.

1. Introduction and background

Supercells moving leftward of the mean wind vector, in the Northern Hemisphere, characteristically contain a mesoanticyclone (after Davies-Jones 1986) that may be treated as the conceptual mirror image of its right-moving counterpart. Cyclonic storms overwhelmingly dominate the literature on supercell conceptualization and processes (i.e., Moller et al. 1994); however, left-moving supercells often produce damaging wind and may rarely spawn tornadoes (i.e., Monteverdi et al. 2001; Dostalek et al. 2004; Edwards et al. 2004). The dominant threat with anticyclonic supercells, however, is large hail. They often produce significant (>5 cm) hail, particularly in environments characterized by large vertical shear and buoyancy, which also support extremely large, damaging hail from right-moving supercells (i.e., Mathews and Turnage 2000; Edwards et al. 2004).

Corresponding author address: Roger Edwards, Storm Prediction Center, National Weather Center, 120 Boren Blvd. #2300, Norman, OK 73069.
E-mail: roger.edwards@noaa.gov

Many left movers are observationally documented (i.e., Nielsen-Gammon and Read 1995) to have developed from the storm splitting process similar to those ideally depicted in numerical models (i.e., Klemp and Wilhelmson 1978; Weisman and Klemp 1982). By contrast, our operational experience, as well as the Sunnyvale, California, example in Monteverdi et al. (2001), indicate that some anticyclonic supercells form discretely, then deviate to the left of the mean shear and/or mean wind soon after genesis.

Here we examine an anomalously intense, anticyclonic supercell affecting a relatively remote area around Aroya, in Lincoln and Cheyenne Counties, Colorado, on the afternoon of 15 June 2002. The supercell produced hail up to 5 cm in diameter, accumulating up to 10 cm deep. This storm is documented and analyzed using multiple observational platforms, including satellite imagery, radar imagery, and field photography (i.e., Fig. 1; discussed in more detail in section 4). The storm's evolution and morphology are examined and compared across both remotely sensed and directly observed perspectives. This is a common general theme for observational studies of cyclonic supercells (i.e.,

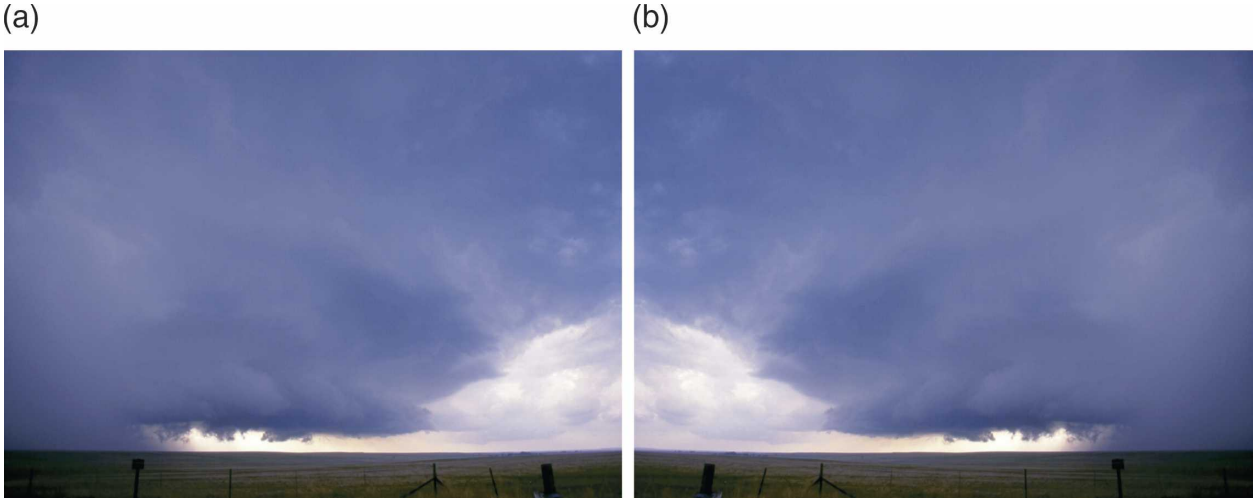

FIG. 1. Direct comparison of observational imagery, in actual and mirrored forms, of an anticyclonic supercell within a period of less than 10 min on 16 Jun 2002: (a) scanned 35-mm transparency photograph, looking northwest from 1.6 km southwest of Aroya, at approximately 0025 UTC; (b) mirror image of (a), which would look southwest if also mirroring the direction of view relative to storm motion; (c) reflectivity image from PUX WSR-88D, located southwest of the image, using 0.5° beam elevation at 0019 UTC; (d) mirror image of (c), with radar located northwest in mirrored form; (e) storm-relative velocity image from PUX at 0.5° beam elevation at 0019 UTC; (f) mirror image of (e), with radar located northwest in mirrored form; (g) mirrored, anticyclonic, color-enhanced adaptation of the planar supercell schematic in Lemon and Doswell's (1979) Fig. 7, where RFD is the rear-flank downdraft, UD is the updraft, and FFD is forward-flank downdraft; and (h) unmirrored (cyclonic) version of (g). Reflectivity imagery is coded according to the embedded table in dB*Z*. Velocity imagery follows embedded table in kt (1 kt = 0.5144 m s^{-1}). Field photograph copyright by R. Edwards, used by permission.

Dowell and Bluestein 2002; Wakimoto and Martner 1992; Bluestein et al. 1989), but not for left movers.

Ground photography, temporally concurrent radar imagery of the storm at peak intensity, and a simple conceptual diagram are presented, inverted into mirror images (Fig. 1) and compared with similar imagery of a cyclonic supercell, for utility in both conceptual relation and in visual recognition by storm spotters. We observationally illustrate a persistent and anomalously intense mesoanticyclone in this storm during the period of its most deviant leftward motion. Observational data and the Rapid Update Cycle (RUC) model soundings (Thompson et al. 2003) are used to evaluate the near-storm environment and assess the predictability of its unusual, east-southeastward average motion for a left-moving supercell. The environment—both in storm-relative and Galilean-invariant frameworks—changed rapidly before storm initiation from one favoring right-moving supercells to one favoring left movers. We illustrate the associated effects on vertical shear and buoyancy related to the combined passage of a cold front and subsequent convective outflow, each prior to the storm's genesis. Finally, this event is used to reinforce the benefits of multiplatform observations of severe local storms and their environments, including the presence of field observers in sparsely populated areas.

2. Documentation and morphology

The Aroya storm developed discretely, not as a result of any storm splitting processes. The first convective towers associated with this cell were evident on visible satellite imagery (Fig. 2) over west-central Lincoln County, Colorado, at about 2230 UTC. Initial reflectivity appeared aloft around 2303 UTC (Fig. 3) on the 3.4° tilt from the WSR-88D radar at Pueblo, Colorado (PUX). This storm then followed a winding, 80-km-long, roughly east-southeastward track. The path consisted of four sharply defined motion stages, for approximately 2.5 h across Lincoln and Cheyenne Counties before dissipating (Fig. 4).

The echo initially moved southeast (from 335°) at 9 m s^{-1}, slower than and slightly to the right of the southeastward mean wind[1] vector, which was from 310° at 12 m s^{-1}. The nascent supercell then became nearly stationary for about 0.5 h, beginning at 2328 UTC. During this phase it interacted with and nearly was absorbed into a previously stronger thunderstorm to the southeast (west-southwest of Boyero, Colorado, in Fig. 3).

[1] In this case, "mean wind" denotes a pressure-weighted averaging of the flow from the level of free convection to the equilibrium level.

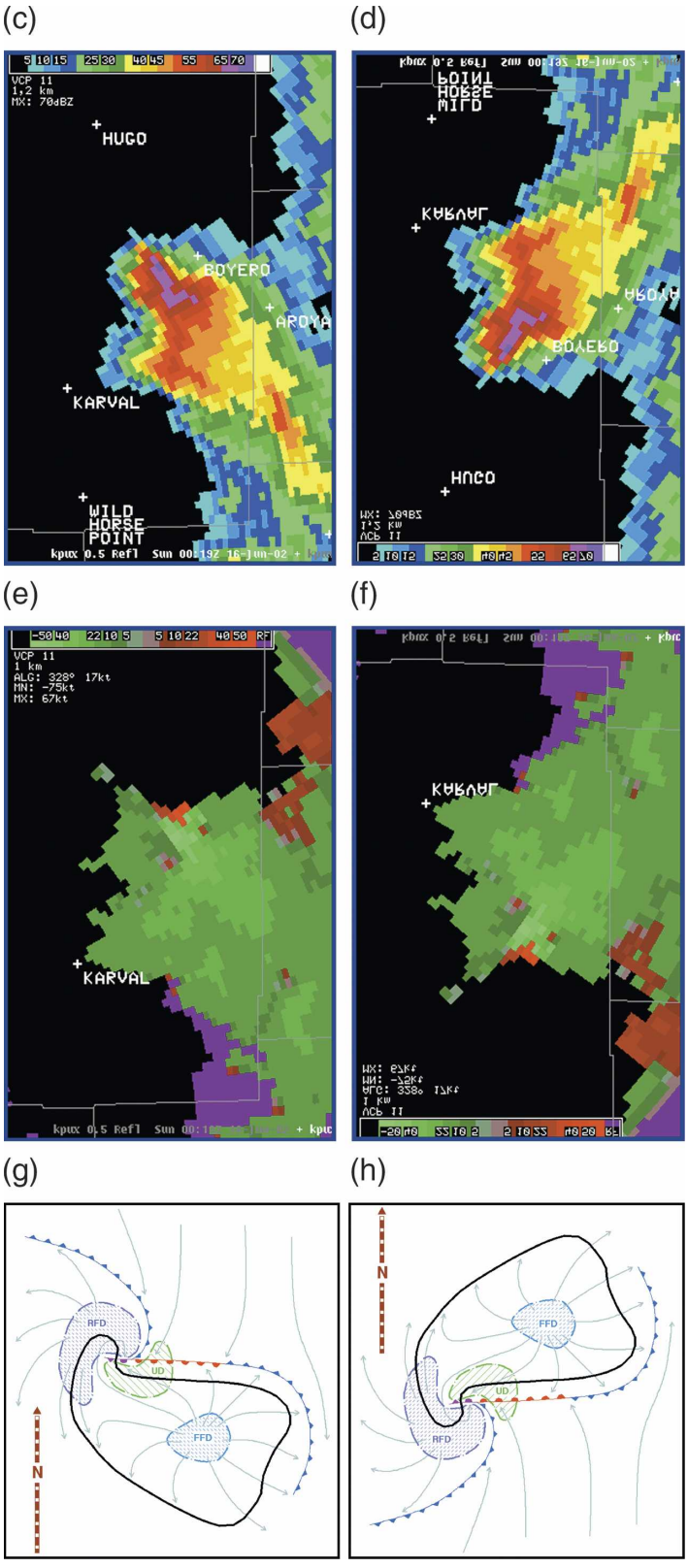

FIG. 1. (*Continued*)

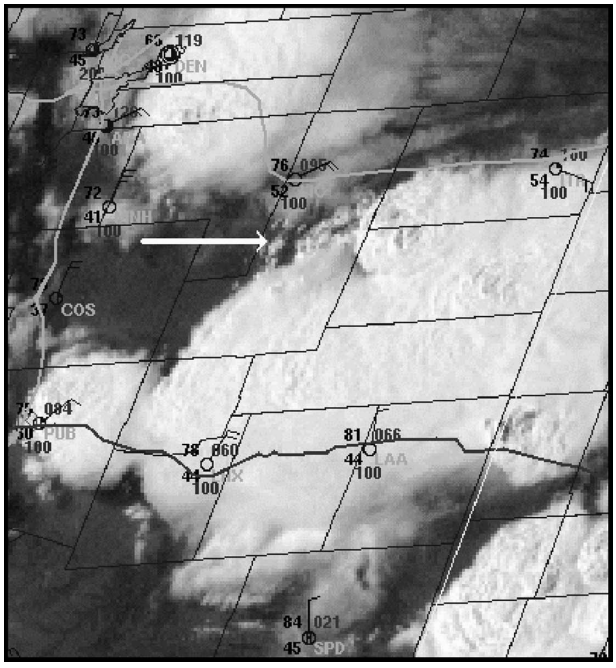

FIG. 2. Geostationary Operational Environmental Satellite visible satellite image over eastern CO at 2232 UTC 15 Jun 2002, with county borders, conventional surface plot, and highway routes overlaid. Arrow indicates convective tower associated with genesis of left-moving supercell.

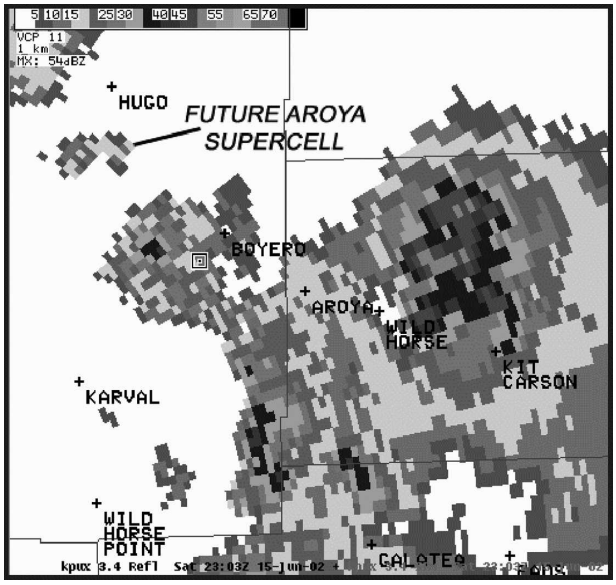

FIG. 3. Reflectivity image at 3.4° beam tilt elevation from PUX at 2303 UTC 15 Jun 2002, denoting the initial echo of the Aroya storm. The 0.5° echo centroid appeared at 2308 UTC (Fig. 4) and was displaced slightly farther south because of tilting of the convective column. Values are scaled in the table and as monochrome versions of those in Fig. 1c.

The two storms' reflectivity patterns merged to the extent that at 2348 UTC their cores—though still discretely recognizable—were separate only at reflectivities >50 dB*Z*. The southern storm's core weakened as the Aroya storm began to move again. The latter accelerated and turned sharply to the left, moving eastward (from 270°) at 10 m s^{-1} toward both the Cheyenne County line and the nearby country crossroads representing the former settlement of Aroya. Meanwhile, the southern storm became better separated until it dissipated at roughly 0045 UTC 16 June.

During the mature phase of most deviant leftward motion, the Aroya storm developed a pronounced mesoanticyclone (Fig. 5) and a northward-tilting, front-flank reflectivity overhang (Fig. 6). These formed mirror images of two characteristics associated for decades with mature cyclonic supercells (i.e., Lemon and Doswell 1979). The mesoanticyclone persisted with uncommon strength for a left mover, based on operational monitoring experience. Initial anticyclonic shear became apparent in storm-relative motion (SRM) data at 0014 UTC 16 June, at a 0.5° elevation angle from PUX.

The storm's anticyclonic vortex remained most strongly evident at the 0.5° beam tilt angle, from both PUX and Goodland, Kansas (GLD), radars. The associated shear couplet weakened with height but extended to between 2.4° and 3.4° elevation, as sensed by each radar (not shown). The mesoanticyclone[2] deepened vertically and strengthened until reaching a peak azimuthal intensity of at least 50 m s^{-1} from PUX at 0034 UTC (Fig. 5a), representing roughly 25 m s^{-1} outbound and inbound SRM values across adjacent gates at the resolution of the display. A similarly intense, but more convergent anticyclonic signature, was evident simultaneously from GLD (Fig. 6b). Peak azimuthal speed differences of 40–50 m s^{-1} were evident at each 5-min interval through 0100 UTC as the storm passed over Aroya and began to turn southeast. This represents at least 45-min duration of >40 m s^{-1} anticyclonic strength associated with this supercell's circulation.

The lead author intercepted and photographed the supercell during this peak phase (i.e., Fig. 1). Relatively hard, smoothly surfaced, spherical hail up to 5 cm in diameter was observed in the forward (southeast) precipitation flank, which damaged the observing vehicle and which was reported to National Weather Service

[2] Throughout much of this interval of greatest leftward deviance, some portions of the storm were mired intermittently in range-folded data voids and/or dealiasing errors at the lowest elevation from PUX and/or Goodland, Kansas; so mesoanticyclonic continuity is inferred from a blend of all available elevation segments of each site's SRM depictions.

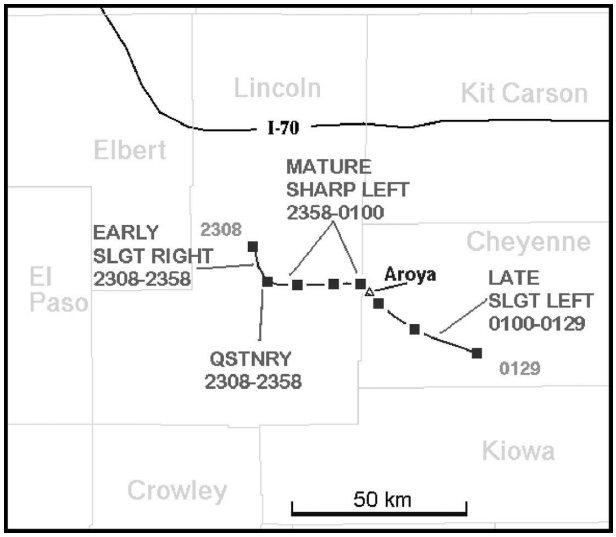

FIG. 4. Track of 0.5° reflectivity centroid for the Aroya supercell over eastern CO. Times are labeled in UTC. Unlabeled points are every three volume scans (approximately 15 min) apart. Area counties, Aroya, and Interstate 70 are designated. The four distinct storm motion and morphology stages, as described in the text, are annotated.

(NWS) warning offices at Boulder, Colorado, and Goodland. There also was distinct visual evidence of low-level clockwise rotation in the relatively precipitation-free updraft region of the storm as the mesoanticyclone approached and passed immediately north through east of a stationary viewing position 1.6 km southwest of Aroya. Hailstones began to fall beneath the updraft region at about 0100 UTC, while continuing from both the forward-flank (east) and the rear-flank (west) downdrafts on either side of the mesoanticyclone. The hail remained roughly constant in distribution, maximum size, and texture throughout the storm-relative (but stationary in ground speed) transect; however, accompanying rainfall diminished markedly from the forward flank through the south rim of the mesoanticyclone. Surface precipitation remained largely hail from that position into the rear-flank precipitation wrapping around the upshear side of the mesocyclone and was accompanied by intermittent light rain and drizzle. The hail accumulated to a depth of up to 10 cm over several square kilometers of short-grass rangeland southwest of Aroya.

As more hail was observed around the updraft base, the storm turned and accelerated east-southeastward, moving from 280° at 17 m s^{-1}. During this fourth motion phase—still to the left of the mean wind—the storm weakened, as evident visually and in reflectivity and SRM trends (not shown), and it dissipated by about 0130 UTC in southern Cheyenne County.

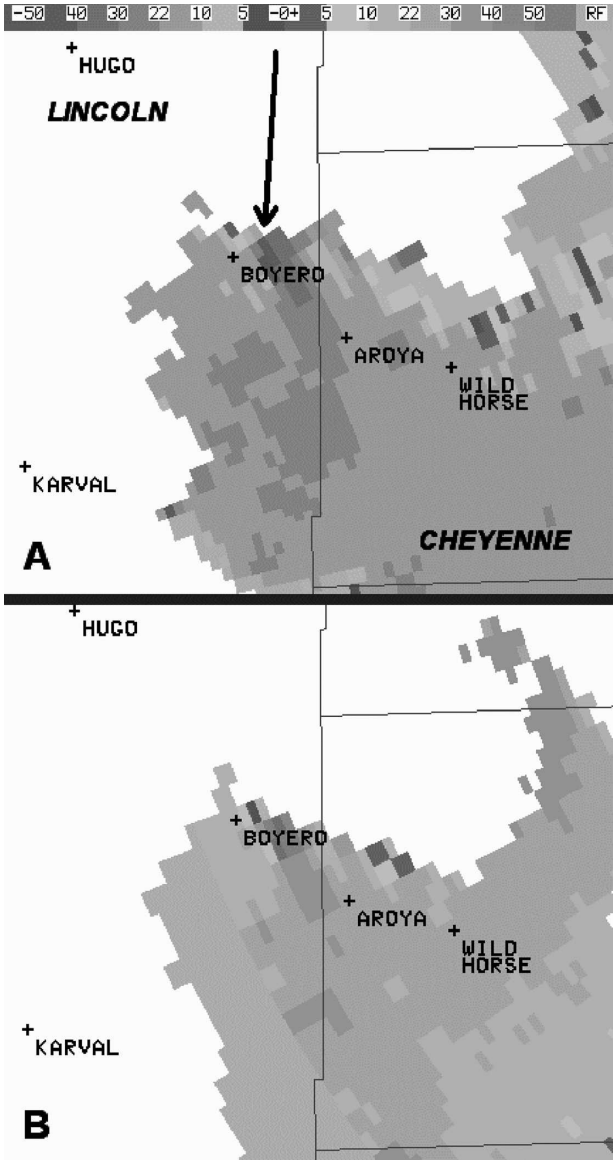

FIG. 5. The 0.5° elevation angle SRM displays at 0034 UTC 16 Jun 2002, from (a) PUX and (b) GLD. County names, arrow pointing toward mesoanticyclone center, and the velocity gray-scale each are provided in (a). Locality names appear on both images, which are scaled identically. PUX and GLD radars were located generally southwest of (a) and northeast of (b), respectively. Velocities are shown in kt (1 kt ≈ 0.5144 m s^{-1}).

3. Environmental overview

Subjective upper-air analyses were performed at 250-, 500-, 700-, and 805-hPa pressure levels for a full suite of synoptic rawinsonde data at 1200 UTC 15 June and 0000 UTC 16 June. (The 805-hPa level was used instead of the more common 850-hPa operational standard because the latter is slightly underground across much of the area. Given the ground elevation of 1500–

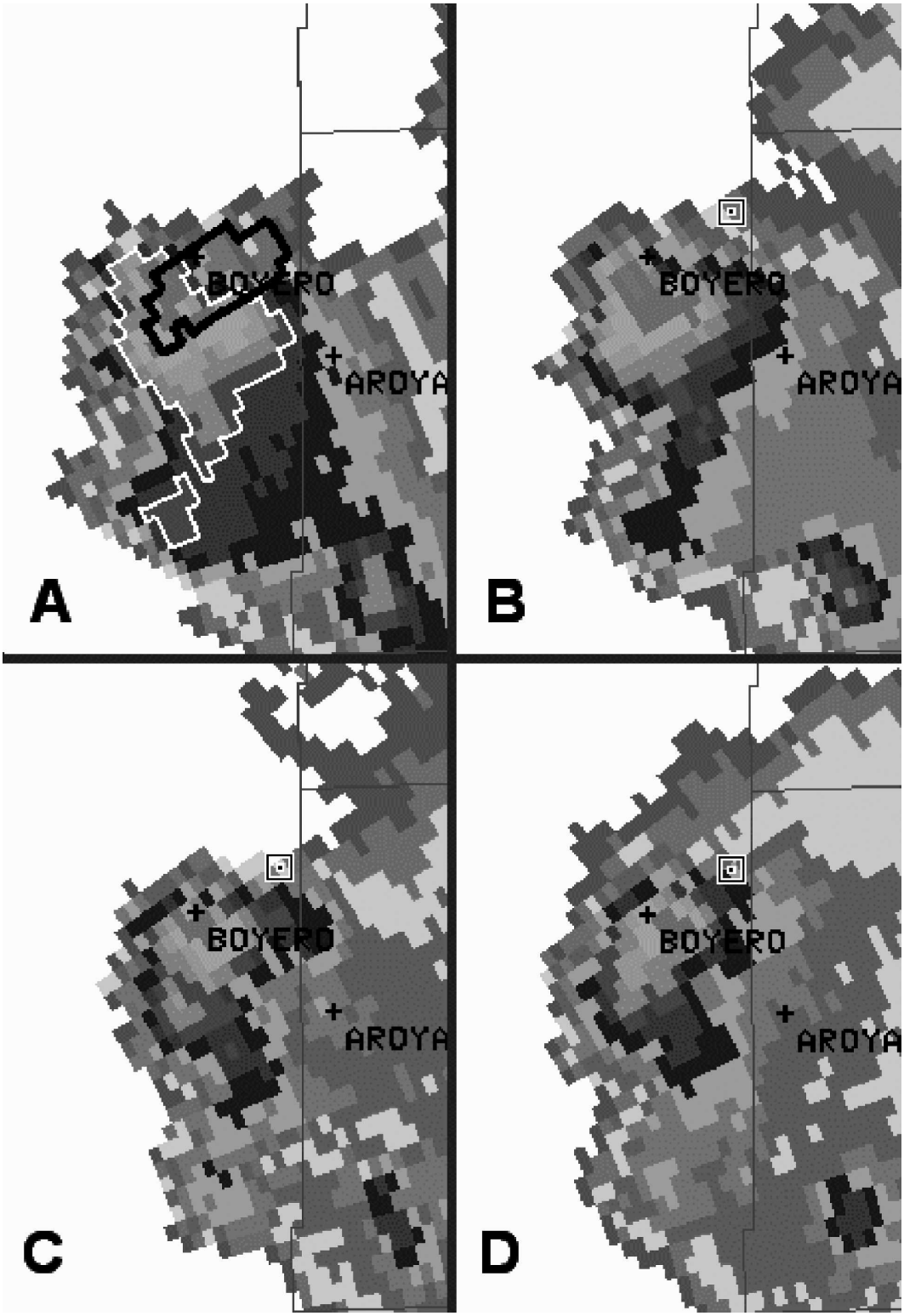

FIG. 6. Reflectivity images from PUX at (a) 0.5°, (b) 1.5°, (c) 2.4°, and (d) 3.4° elevation angles, following intensity and mapping conventions of Fig. 1c. Spatial scale is identical for each panel. For illustrating the reflectivity overhang, the thin white line in (a) represents the outline of the ≥45 dBZ reflectivity contour at that level, while the thick black outline is of the ≥45 dBZ isopleth in (d).

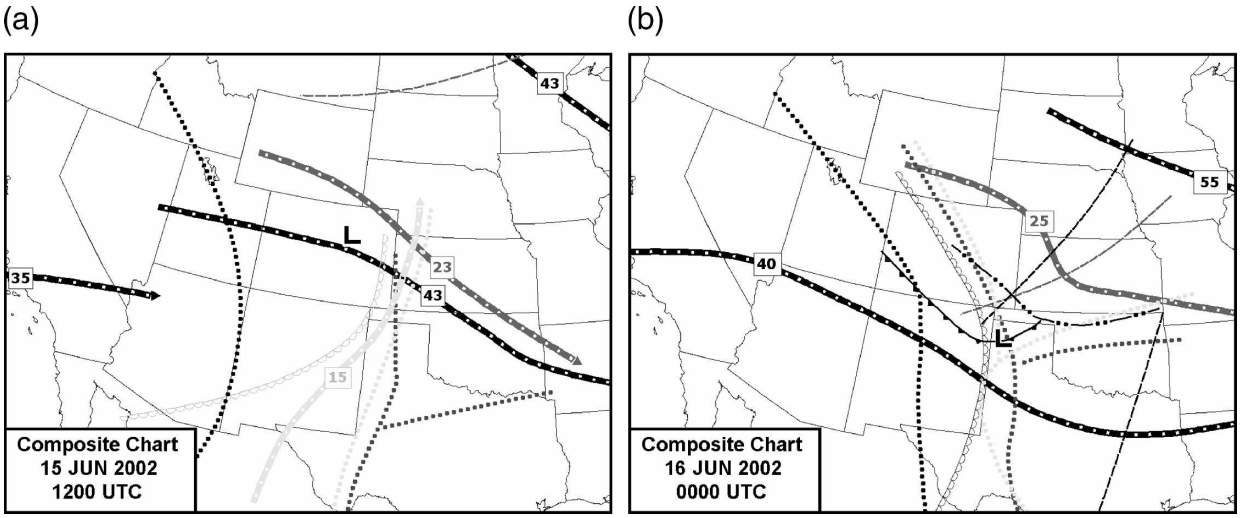

FIG. 7. Composite charts as labeled. Thick black (medium gray) lines denote 250-hPa (500-mb) jets with speed maxima marked in m s^{-1}. Thin dark (medium gray) lines are 250- (500-) hPa height troughs. Dotted gray lines represent moist axes at 700 (dark) and 805 hPa (light), respectively. Scalloped gray line collectively represents the 700- and 805-hPa drylines, which were practically juxtaposed at each analysis time. Dotted black line is the 805-hPa thermal axis. Surface features (low, cold front, and outflow boundary) are conventionally drawn in black.

2000 m MSL in this area, the 805- and 700-hPa levels may serve as a coarse proxy for the 925- and 850-hPa mandatory levels over the low plains farther east.) Also examined were special soundings launched at 1500, 1800, and 2100 UTC, at the usual National Weather Service sounding locations across the Great Plains, in support of the International H2O Project (IHOP). These data (not shown) were blended with hourly plots of profiler winds, WSR-88D velocity azimuth display wind profiles (VWP), and surface observations for composite analyses. Results are summarized graphically as composite charts in Fig. 7.

The area was under a general northwest flow regime aloft, characterized at 1200 UTC by a roughly 35–45 m s^{-1} 250-hPa jet and a weak 500-hPa trough located well to the north from northern Minnesota to Montana. By 1800 UTC, regional profiler winds and the intermediate sounding at Denver, Colorado (not shown), indicated that this trough had reached extreme north-central Colorado, south-central Wyoming, and western Nebraska. By 0000 UTC 16 June, the trough had moved to southeastern Nebraska, central Kansas, and extreme southeastern Colorado. The trough's proximity to eastern Colorado was well timed to vertically juxtapose with peak insolation-related heating of the boundary layer air mass along and behind a surface cold front. This appeared to contribute to steepened lapse rates, based on modified RUC soundings and time series comparisons of 1200, 1800, and 0000 UTC rawinsonde soundings. The low-level dryline had retreated across Colorado through the day, a process aided by weak moist advection behind the front.

At the surface, only broad, weak baroclinicity was evident across the central high plains at 1200 UTC, with a weak surface low near Limon, Colorado. By 1500 UTC, a surface low was analyzed over Akron, Colorado, with a weak cold front developing southwestward to near Limon, then westward to near Monument, Colorado. By 1800 UTC, the frontal low had become ill defined, and another had formed near Pueblo at a surface thermal maximum. The cold front then was crossing a broad, zonally oriented, topographic ridge near Limon known as the Palmer Divide, as well as the I-70 corridor near the Kansas border. The front continued southward through the Arkansas River valley of southeastern Colorado around 2100 UTC, and then by 0000 UTC 16 June into northeastern New Mexico (Fig. 7).

Thunderstorms developed in locations along and behind the surface cold front throughout the day, beginning as early as 1500 UTC to the south of Akron, and around 1800 UTC along the Palmer Divide. Associated cloud and precipitation coverage became more widespread from the Palmer Divide southward and southeastward through the afternoon, as observed visually from the ground and on radar and satellite imagery. The aggregate outflows modified the surface air to be substantially colder than the ambient postfrontal air mass. By 2100 UTC, temperatures immediately behind the front in southeastern Colorado remained in the 28°–30°C range, while temperatures in the postfrontal

outflow air were falling generally into the 24°–26°C range. By 0000 UTC the difference was even more pronounced, with outflow air as cold as 19°C over easternmost Colorado near Burlington, and postfrontal temperatures of 29°–32°C near the southeast corner of Colorado.

The Aroya supercell developed well north of the surface cold front and outflow boundary, along the northwest periphery of a large complex of thunderstorms that covered much of southeastern Colorado (evident in visible imagery, Fig. 2). No boundaries or other distinct convective foci were evident either in surface analyses, reflectivity, or satellite data at the genesis location, which was along the Palmer Divide. Differential heating of locally elevated terrain and associated solenoidal ascent along the edge of the large anvil canopy *may have contributed* to this storm's origin in a weakly capped environment, based on a lifted RUC surface parcel (Fig. 8a). Alternatively, an outflow boundary from the large area of convection to the south may have aided initiation of the Aroya storm. Observational data coverage is insufficient to verify either process, however.

Hourly RUC model soundings have been shown to reliably represent the environments of discrete supercells (Thompson et al. 2003). Here, the 0000 UTC June 16 RUC analysis point forecast sounding for Limon (Fig. 8a) closely approximated surface thermodynamic conditions observed both at Limon and in the immediate vicinity of the storm. The RUC sounding was judged to be the most representative of conditions ambient to this storm, by comparison with the 1800 UTC June 15 and 0000 UTC June 16 Denver rawinsonde soundings, forecast soundings from the 1800 UTC Eta model, and initialized 0000 UTC Eta model soundings (not shown).

Our initial hypothesis was that this storm was elevated atop cold air from the north side of the front that had been further reinforced by outflows. However, further examination indicates that the storm probably was surface based, despite the postfrontal and postconvective environment characterized by "cool" 20°–21°C inflow air temperatures, as measured in situ by the lead author and as observed at Limon, 40 mi (65 km) to the northwest. Surface-based CAPE using the virtual temperature correction (Doswell and Rasmussen 1994) was estimated to be nearly 1500 J kg^{-1} based on the RUC sounding, amidst roughly 8°C km^{-1} midtropospheric lapse rates.

During its anticyclonic rotation phase, the supercell moved leftward of both the mean wind and mean shear vectors and the hodographs through 0–1 and 0–3 km above ground level (AGL). This is consistent with negative values of storm-relative helicity (SRH) expected and commonly documented for surface-based left movers (i.e., Bunkers 2002; Edwards et al. 2004). However, the 0–1- and 0–3-km AGL SRH for this case—given any of the four dominant motion vectors in its lifespan—was considerably larger in magnitude and more negative than averages or medians for the Bunkers (2002) or Edwards et al. (2004) datasets of left-moving supercells. During the mature, eastward-moving phase near Aroya, the RUC hodograph, modified with input from the observed storm motion, yielded 0–1-km (0–3-km) net SRH of $-363\ m^2\ s^{-2}$ ($-421\ m^2\ s^{-2}$). Among favorable Galilean-invariant parameters for supercells were 24 m s^{-1} speed shear through the 0–6-km AGL layer and 59 $m^2\ s^{-2}$ bulk Richardson number shear (each after Weisman and Klemp 1982).

4. Visual characteristics

Cloud and precipitation debris from other convection (evident east of the Aroya storm in Figs. 1 and 2) obscured the view of the supercell upon ground-level approach from the Lamar, Colorado, area to the southeast. As the storm came into view from near Aroya, it exhibited (in mirror image) classical supercell structures (e.g., Lemon and Doswell 1979) with a rain-free base, striated low–middle-level cloud decks, and pronounced forward-flank precipitation core.

To better aid conceptualization of this structure for storm spotters and other observers, the photograph of this storm near peak intensity, showing these structures, is flipped into a mirror image in Fig. 1. Given the storm's overall motion toward the east-southeast, a mirror for the spotting angle would be for a storm moving toward the east-northeast.

Although this storm was nontornadic, the visual mirror image of its cloud features bore striking structural resemblance to a cyclonic, tornadic supercell on 4 October 1998 near Dover, Oklahoma, as evident in Fig. 9. The Dover storm was within 3 min of producing a tornado from the lowest portion of the cloud base at left, an area which was beginning to exhibit strong, concentrated, cyclonic rotation at the time of the photo. By contrast, only weak, broad cloud-base rotation was evident in the Aroya storm from the time of the photograph until it passed overhead (at the same vantage point); and a tornado never appeared imminent. The intense shears detected in middle levels of the storm, as shown in Fig. 5, were not visually evident lower in the storm and at cloud base.

5. Summary and discussion

This event illustrates that the anticyclonic supercell, when observable in the field and remotely with radar,

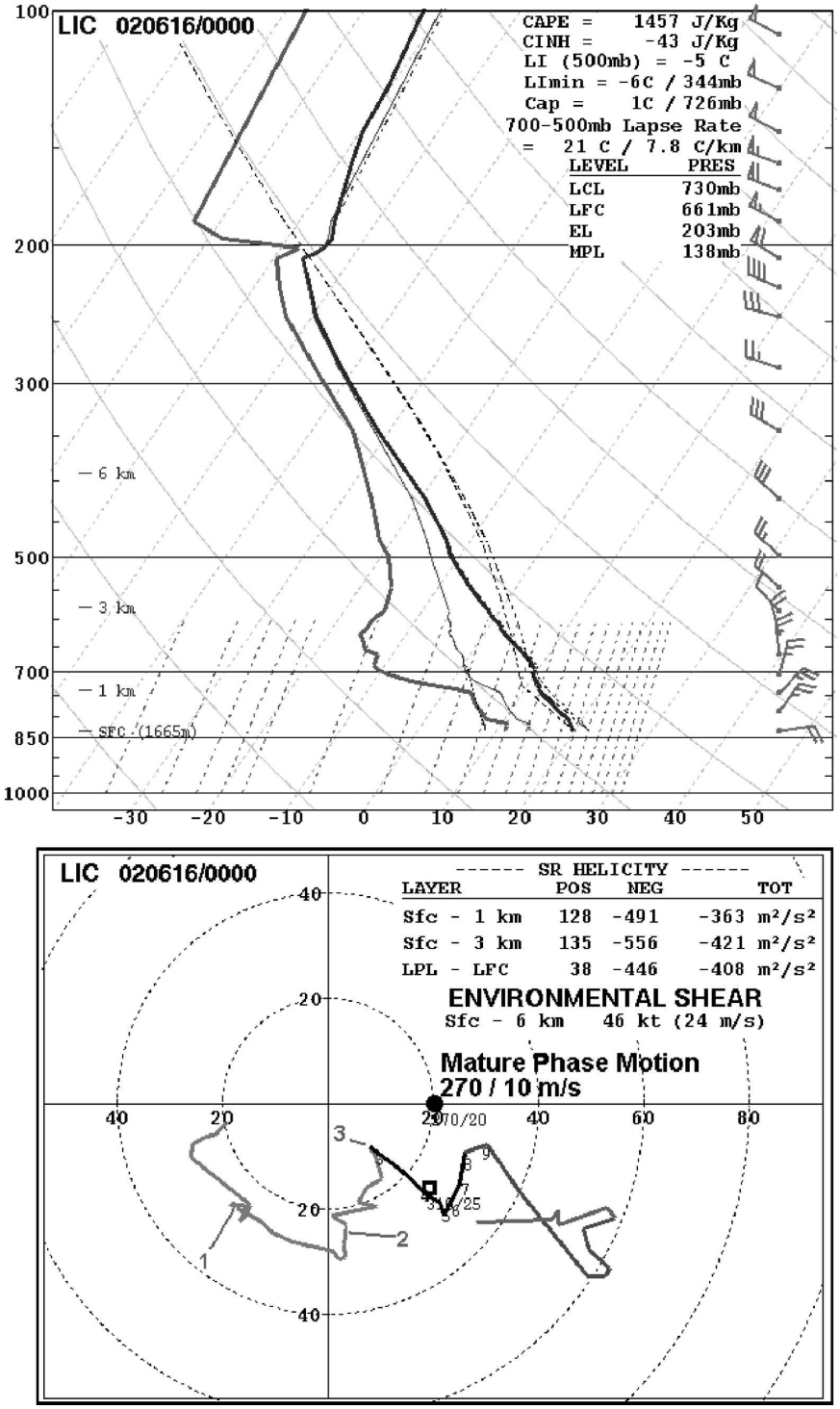

FIG. 8. RUC model initial sounding for Limon, at 0000 UTC 16 Jun 2002, plotted as a (top) skew-T diagram and (bottom) hodograph, with annotated parameter values on each. Wind barbs (flags) represent 5 (25) m s^{-1} speeds. On the hodograph, isotachs are labeled in kt but with mature phase storm speed noted at 10 m s^{-1}, and heights from 1 to 3 km are labeled.

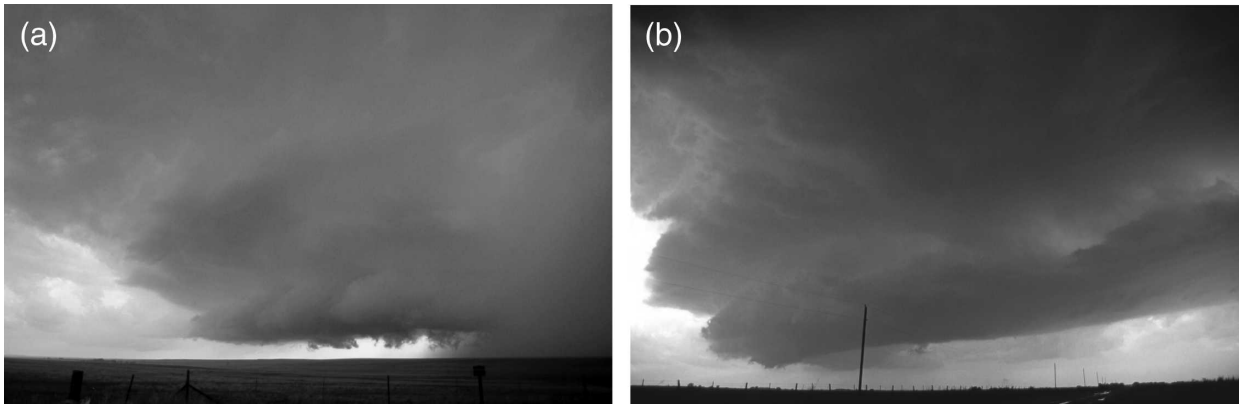

FIG. 9. Visual storm structure comparison using monochrome photographs of (a) the nontornadic, anticyclonic Aroya supercell from 15 Jun 2002, mirrored as if to look toward the southwest, and (b) the incipiently tornadic, cyclonic Dover supercell of 4 Oct 1998, with actual view to the southwest.

may be treated as a visual and conceptual mirror image of the cyclonic supercell (Fig. 1) for application to spotter training and for basic-level conceptual understanding of its structure and morphology.

This case also shows that environments behind both cold fronts and reinforcing convective outflows still may support supercells with significant severe weather, that is, the 5-cm hail occurring in this event. The ambient vertical wind profile was typical for a cold advection regime in that the direction of flow backed with height, which also is an ideal wind profile for large negative SRH given an embedded, left-moving storm. Left movers are probably not as common as right-moving supercells because of this association with cold advection and the detrimental effect that such cooling can have on buoyancy, though dominant left movers also may occur in wind profiles that veer with height. However, this event illustrates that, to the extent that the RUC sounding was representative of the environment, surface-based CAPE was more than adequate to support severe convection, despite the presence of postfrontal, postconvective cold-air advection in the boundary layer. Adjusting for the context of left movers, this reinforces the concept of favorable surface-based buoyancy on the "cold" side of baroclinic boundaries [e.g., Verifications of the Origins of Rotation in Tornadoes Experiment (VORTEX) findings of Markowski et al. 1998]—whether storms cross such a boundary or, as in this event, initiate well behind it.

One important question that may be substantively unanswerable for this case, given 1) its surface-based nature and 2) its long-lived, intense mesoanticyclone is the following: Why did this storm not produce a tornado? Tornadic left movers have been documented (i.e., Monteverdi et al. 2001; Dostalek et al. 2004) in environments with only about 500 J kg^{-1} more CAPE and weaker SRH. More detailed and dense field observations, as have been performed in field experiments such as VORTEX, might contribute to a better understanding of the difference between tornadic and nontornadic processes in left movers as well. Furthermore, we recommend algorithmic indication and tracking of mesoanticyclones in WSR-88D operations, analogous to that of mesocyclones, for similar benefits to both warning operations and climatological research on the phenomenon. Another question for investigation is, why do so few anticyclonic supercells produce tornadoes compared to cyclonic storms?

IHOP intermediate soundings, in combination with profiler and VWP data and hourly RUC soundings, were useful in assessing the thermodynamic and kinematic evolution of features above the surface throughout the day, in between synoptic balloon launches. Intermediate rawinsonde launches often are requested regionally by Storm Prediction Center forecasters on days of exceptional concern; and this case emphasizes the benefit of both asynoptic observed soundings and RUC hourly model soundings. This study also underscores the need for subjective analysis and detailed utilization of multiple platforms therein. The subtle and still poorly understood character of initiation foci for convection north of the cold front supports the need for more dense surface data of the sort provided by the Oklahoma Mesonet (Brock et al. 1995), benefiting both postmortem research and real-time operational forecasting of meso-β- and smaller-scale convective processes.

Storm observation in the field remains an immeasurably valuable tool in assessment and verification of severe weather events. Several spotters and storm chasers contributed severe weather information, both in real time and post facto, to the jurisdictional NWS warning offices in Boulder and at Goodland. Without their pres-

ence in this event and in others in the sparsely populated Great Plains, neither precise and accurate watch and warning verification nor field documentation such as that herein would be as common. The phenomenon of low population density has handicapped efforts to improve radar-based warning algorithms and operations, with various statistical or geographical adjustment methods devised to compensate (i.e., Witt et al. 1998; Lenning et al. 1998). Low population affects severe weather climatology as well. Observed severe weather report collections for other sparsely populated parts of the Great Plains have sometimes been statistically modulated by up to tenfold multiples, as in the nontornadic severe weather climatology of Paruk and Blackwell (1994). By at least transiently populating the landscape around severe storms, some of these impacts may be ameliorated.

Furthermore, documentation resulting from field observations—including still photography and video—is used commonly for subsequent spotter training. A responsible and well-trained fleet of spotters and mobile storm chasers has been demonstrated, in many instances (i.e., Pietrycha and Fox 2004; Moller et al. 1994, Winston 1988), to benefit both real-time warning operations and subsequent research and verification efforts, and should be encouraged and supported wherever possible.

Acknowledgments. The authors thank Paul Wolyn of NWS Pueblo, along with NWS Central Region and the SPC Scientific Support Branch, for generously supplying data and platforms for analysis both at Pueblo and Norman. Thanks to Elke Edwards for her skilled intercept navigation and to Al Pietrycha for his excellent nowcasting, both of which made close observation and documentation of this storm possible from afield. Steve Weiss (SPC) provided very helpful encouragement, guidance, and internal review. We deeply appreciate the formal reviewers for their beneficial comments and suggestions for revision.

REFERENCES

Bluestein, H. B., E. W. McCaul Jr., G. P. Byrd, G. R. Woodall, G. Martin, S. Keighton, and L. C. Showell, 1989: Mobile sounding observations of a thunderstorm near the dryline: The Gruver, Texas storm complex of 25 May 1987. *Mon. Wea. Rev.,* **117,** 244–250.

Brock, F. V., K. C. Crawford, R. L. Elliott, G. W. Cuperus, S. J. Stadler, H. L. Johnson, and M. D. Eilts, 1995: The Oklahoma Mesonet: A technical overview. *J. Atmos. Oceanic Technol.,* **12,** 5–19.

Bunkers, M. J., 2002: Vertical wind shear associated with left-moving supercells. *Wea. Forecasting,* **17,** 845–855.

Davies-Jones, R. P., 1986: Tornado dynamics. *Thunderstorm Morphology and Dynamics,* 2d ed., E. Kessler, Ed., University of Oklahoma Press, 197–236.

Dostalek, J. F., J. F. Weaver, and G. L. Phillips, 2004: Aspects of a tornadic left-moving thunderstorm on 25 May 1999. *Wea. Forecasting,* **19,** 614–626.

Doswell, C. A., III, and E. N. Rasmussen, 1994: The effect of neglecting the virtual temperature correction on CAPE calculations. *Wea. Forecasting,* **9,** 625–629.

Dowell, D. C., and H. B. Bluestein, 2002: The 8 June 1995 McLean, Texas, storm. Part II: Cyclic tornado formation, maintenance, and dissipation. *Mon. Wea. Rev.,* **130,** 2649–2670.

Edwards, R., R. L. Thompson, and C. M. Mead, 2004: Assessment of anticyclonic supercell environments using close proximity soundings from the RUC model. Preprints, *22d Conf. on Severe Local Storms,* Hyannis, MA, Amer. Meteor. Soc., CD-ROM, P1.2.

Klemp, J. B., and R. B. Wilhelmson, 1978: Simulations of right- and left-moving storms produced through storm splitting. *J. Atmos. Sci.,* **35,** 1097–1110.

Lemon, L. R., and C. A. Doswell III, 1979: Severe thunderstorm evolution and mesocyclone structure as related to tornadogenesis. *Mon. Wea. Rev.,* **107,** 1184–1197.

Lenning, E., H. E. Fuelberg, and A. I. Watson, 1998: An evaluation of WSR-88D severe hail algorithms along the northeastern Gulf Coast. *Wea. Forecasting,* **13,** 1029–1044.

Markowski, P. M., E. N. Rasmussen, and J. M. Straka, 1998: The occurrence of tornadoes in supercells interacting with boundaries during VORTEX-95. *Wea. Forecasting,* **13,** 852–859.

Mathews, G. N., and T. J. Turnage, 2000: An example of a left-split supercell producing 5-inch hail: The Big Spring, Texas, storm of 10 May 1996. Preprints, *20th Conf. on Severe Local Storms,* Orlando, FL, Amer. Meteor. Soc., 526–529.

Moller, A. R., C. A. Doswell III, M. P. Foster, and G. R. Woodall, 1994: The operational recognition of supercell thunderstorm environments and storm structure. *Wea. Forecasting,* **9,** 327–347.

Monteverdi, J. P., W. Blier, G. J. Stumpf, W. Pi, and K. Anderson, 2001: First WSR-88D documentation of an anticyclonic supercell with anticyclonic tornadoes: The Sunnyvale–Los Altos, California, tornadoes of 4 May 1998. *Mon. Wea. Rev.,* **129,** 2805–2814.

Nielsen-Gammon, J. W., and W. L. Read, 1995: Detection and interpretation of left-moving severe thunderstorms using the WSR-88D: A case study. *Wea. Forecasting,* **10,** 127–140.

Paruk, B. J., and S. R. Blackwell, 1994: A severe thunderstorm climatology for Alberta. *Natl. Wea. Dig.,* **19,** 27–33.

Pietrycha, A. E., and M. Fox, 2004: Effective use of various communication methods during a severe convective outbreak. *Natl. Wea. Dig.,* **28,** 59–64.

Thompson, R. L., R. Edwards, J. A. Hart, K. L. Elmore, and P. M. Markowski, 2003: Close proximity soundings within supercell environments obtained from the Rapid Update Cycle. *Wea. Forecasting,* **18,** 1243–1261.

Wakimoto, R. M., and B. E. Martner, 1992: Observations of a Colorado tornado. Part II: Combined photogrammetric and Doppler radar analysis. *Mon. Wea. Rev.,* **120,** 522–543.

Weisman, M. L., and J. B. Klemp, 1982: The dependence of numerically simulated convective storms on vertical wind shear and buoyancy. *Mon. Wea. Rev.,* **110,** 504–520.

Winston, H. A., 1988: A comparison of three radar-based severe storm detection algorithms on Colorado High Plains thunderstorms. *Wea. Forecasting,* **3,** 131–140.

Witt, A., M. D. Eilts, G. J. Stumpf, E. D. Mitchell, J. T. Johnson, and K. W. Thomas, 1998: Evaluating the performance of WSR-88D severe storm detection algorithms. *Wea. Forecasting,* **13,** 513–518.